Available online at www.sciencedirect.com
SCIENCE DIRECT®
Journal of Hydrology 285 (2004) 125–142
Journal of Hydrology
www.elsevier.com/locate/jhydrol

Simulating temporal and spatial variation of evapotranspiration over the Lushi basin

Xingguo Mo[a,*], Suxia Liu[a,b], Zhonghui Lin[a], Weimin Zhao[c]

[a]*Institute of Geographical Sciences and Natural Resources Research, Chinese Academy of Sciences, Beijing 100101, People's Republic of China*
[b]*School of Mathematics, The University of New South Wales, Sydney, NSW 2052, Australia*
[c]*Bureau of Hydrology, Yellow River Conservancy Commission, Zhengzhou 450004, People's Republic of China*

Received 29 May 2001; accepted 4 August 2003

Abstract

A process-based distributed model is established to simulate the temporal and spatial variation of evapotranspiration over the Lushi basin in China. The model components include the parameterization of land surface resistances, energy transfer, soil water movement, interception and surface runoff. What is distinguished in our model is the scheme for evapotranspiration partition by introducing a working variable related to the water vapor deficit at the reference height. The basin was divided into 6227 grids with resolution of 30 × 30 arc seconds. A digital elevation model was used to correct meteorological variables for altitude, and the inverse distance square method was adopted for spatial interpolation of precipitation over the basin. The remotely sensed normalized difference vegetation index (NDVI) in 1996 and the land use/cover data, both with the resolution of 30 × 30 arc seconds, were used to retrieve the distribution of vegetation leaf area index (LAI). The evapotranspiration simulated by using 1996 NDVI-derived LAI is close to that by using phenologically derived LAI. The differences of annual amounts of evapotranspiration from 1984 to 1997 simulated by using LAI derived by 1992, 1995 and 1996 monthly composite NDVI are less than 30 mm yr^{-1} (or 5%), in which 1995 represents drought and 1992 wet. The simulated annual evapotranspiration (E_{Ta}) plus soil storage change from 1984 to 1997 is in good agreement with precipitation minus discharge at the outlet. The spatial pattern of annual evapotranspiration and its components in 1996 clearly corresponded to the precipitation and LAI patterns over the basin. The highest monthly evapotranspiration (E_{Tm}) occurred in the period of July to August with 104 mm $month^{-1}$. The value of E_{Tm} for irrigated farmland is higher than that for other vegetation types all the year and the values of E_{Tm} for grass and arid farmland are similar and about 10 mm $month^{-1}$ higher than those for forest covers in summer. The predicted annual evapotranspiration in 1996 over the Lushi basin is 628 mm with the transpiration 327 mm, soil evaporation 256 mm and canopy interception 45 mm, respectively.

Keywords: Process-based distributed model; Basin evapotranspiration; Remote sensing; Normalized difference vegetation index

1. Introduction

Apart from precipitation and runoff, evapotranspiration is the principal part of a hydrological cycle in semi-humid and arid regions, affected by both

* Corresponding author. Fax: +86-10-851844.
E-mail address: moxg@igsnrr.ac.cn (X. Mo).

0022-1694/$ - see front matter © 2003 Elsevier B.V. All rights reserved.
doi:10.1016/j.jhydrol.2003.08.013

biophysical and environmental processes at the interface between soil, vegetation and atmosphere.

In classic hydrological models, evapotranspiration is always simulated in an empirical or conceptual way (Zhao, 1992), and mostly in a lumped way as in the HEC (Hydrological Engineering Center) model and Tank models (Singh, 1995). As topography, soil characteristics, vegetation, and climate interact in a complex manner to determine the complete hydrological cycle, including runoff production and evapotranspiration, in distributed process-based models it is highly preferable to simulate evapotranspiration and other hydrological processes as a physical process.

Considerable progress has recently been made in the application of process-based soil–vegetation–atmosphere transfer (SVAT) models to simulate evapotranspiration over a basin and global scale (Famiglietti and Wood, 1996; Dawes et al., 1997; Choudhury and Digirolamo, 1998; Strasser and Mauser, 2001). While defining the characteristics of a given basin, process-based models generally need a large number of parameters that are usually heterogeneous and unavailable at an appropriate scale. This is the unfavorable aspect of process-based modeling (Beven, 2001). Significant efforts on the utilization of remote sensing data or the coupling of one-dimensional SVAT models with distributed routing models have remarkably improved the reliability of the simulation results (Liang et al., 1994; Mauser and Schadlich, 1998; Silberstein et al., 2003). But the regionalization of the input data fields as well as the validation of the simulation results still crucially limit the application of such models, especially in regions where data collecting systems are not well established (McVicar and Jupp, 1999).

Given the recent advances in simulating evapotranspiration over basins worldwide, there are still few applications in China. China is now experiencing dramatic land use and land cover changes with its rapid development and high population. The hydrological cycles in many basins of China, especially in the Yellow River basin which is the study area of this paper, have been dramatically changed by human behaviors (Wang and Takahashi, 1999; Liu et al., 2001). It is thus of great importance to assess the basin evapotranspiration and its components with a process-based model for the current state of the land surface and to quantify likely changes in evapotranspiration due to land use/cover change.

The topics of such studies are numerous. The objectives of this paper will be limited: (1) to describe a simplified physically based distributed model for simulation of evapotranspiration over the mid-sized Lushi basin; (2) to capture the basic temporal and spatial characteristics of evapotranspiration over the basin; and (3) to explore the relationship between evapotranspiration and land use.

In this paper, first we briefly describe the model, the Lushi basin and data preparation. The model is run with a continuous, 14-year time-series of meteorological and hydrological input data (1984–1997). In order to test the representation of 1996 normalized difference vegetation index (NDVI) data to all other years from 1984 to 1997, comparison is made between the annual evapotranspiration estimates with both NDVI-derived and phenologically derived leaf area index (LAI) data. In order to validate the model, the annual evapotranspiration simulated by the model is compared with that calculated by the water balance method in the basin. By taking advantage of the distributed process-based model, the relationship between the spatial pattern of annual evapotranspiration and the land vegetation covers is explored in the year 1996. Based on the same year's data, seasonal variation of the evapotranspiration is analyzed. In order to check the validity of model assumptions, parameters sensitivity analysis is done next. Finally, we draw some conclusions.

2. Model description

A simplified parameterization model of SVAT is used in this study, including a two-source canopy energy exchange scheme and a three-layer soil moisture dynamic scheme (Shuttleworth and Wallace, 1985; Sellers et al., 1996). Water and energy balance components are calculated for each cell separately, neglecting flux exchanges between cells. Water supply to irrigated field is assumed to be drawn from rivers in the basin. The grid size is $30'' \times 30''$ (latitude $\times$ longitude). Since the energy fluxes response to the atmospheric driving forces much more quickly than those to hydrological cycle in the soil, in our model, as adopted elsewhere (Silberstein

et al., 2003), the energy budget part will run on hourly, with daily time step for soil moisture balance.

2.1. Estimation of transpiration and soil evaporation

The net radiation above the canopy, R_n, is partitioned into the net radiation absorbed by canopy, R_{nc}, and soil, R_{ns}

$$R_n = R_{nc} + R_{ns} \tag{1}$$

Energy balances for canopy and soil surface are

$$R_{nc} = \lambda(E_c + E_i) + H_c \tag{2}$$

$$R_{ns} = \lambda E_s + H_s + G \tag{3}$$

where E_c, E_i and E_s are the canopy transpiration, direct evaporation from the intercepted water and soil evaporation, respectively. λ is the latent heat of vaporization, H_c and H_s are the canopy and soil surface sensible heat fluxes, respectively, G is the soil heat flux. The two-source scheme of canopy energy balance makes the assumption that there is a source within canopy and the heat and water vapor are exchanged between soil surface, canopy, source and atmosphere above canopy (Shuttleworth and Wallace, 1985). By introducing a working variable of water vapor deficit, D_0, at the source height (Appendix A, in more detail, cf. Mo et al., 2000; Mo and Liu, 2001), λE_c, λE_i and λE_s can be expressed in a similar form to the Penman–Monteith equation as follows

$$\lambda E_c = \frac{\Delta R_{nc} + \dfrac{\rho C_p D_0}{r_{ac}}}{\Delta + \gamma\left(1 + \dfrac{r_c}{r_{ac}}\right)}(1 - W_{fr}) \tag{4}$$

$$\lambda E_i = \frac{\Delta R_{nc} + \dfrac{\rho C_p D_0}{r_{ac}}}{\Delta + \gamma} W_{fr} \tag{5}$$

$$\lambda E_s = \frac{\Delta(R_{ns} - G) + \dfrac{\rho C_p D_0}{r_{as}}}{\Delta + \gamma\left(1 + \dfrac{r_s}{r_{as}}\right)} \tag{6}$$

where ρ is the air density, C_p is the air specific heat at constant pressure, γ is the psychrometric constant, Δ is the first-order derivative of saturation vapor pressure with temperature. W_{fr} is the wetted fraction of the canopy. r_c, r_s, r_{ac} and r_{as} are the canopy resistance, soil resistance, bulk boundary-layer resistance of the canopy and aerodynamic resistance between the soil surface and canopy air space, respectively. While calculating D_0, the aerodynamic resistance between canopy source and reference level, r_a, is also included. The following is the description of all the related resistances.

2.2. Land surface resistance parameterization

2.2.1. Aerodynamic resistance between canopy source and reference level

The aerodynamic resistance between canopy source and reference level, r_a, for heat and vapor transfer between the vegetation surface and the reference height is calculated with an analytical method (Choudhury et al., 1986) for both stable and unstable conditions. For unstable condition, r_a is given by

$$r_a = \log\left(\frac{z-d}{z_{0m}}\right)\log\left(\frac{z-d}{z_{0h}}\right)/\kappa^2 u_a(1+\eta)^2 \tag{7}$$

For stable conditions, r_a is expressed as

$$r_a = \log\left(\frac{z-d}{z_{0m}}\right)\log\left(\frac{z-d}{z_{0h}}\right)/\kappa^2 u_a(1+\eta)^{0.75} \tag{8}$$

where u_a is the wind speed at reference height z, κ is the von-Karman constant, d is the zero displacement height, z_{0m} is the roughness length for momentum transfer, z_{0h} is the roughness length for heat and water vapor transfer, η is the atmospheric stability correction factor.

Usually, d and z_{0m} are estimated from the mean height of canopy, h_c. For crop and grass, it is assumed that $z_{0m} = 0.123h_c$ and $d = 0.67h_c$ (Monteith, 1981). For forest, it is assumed that $z_{0m} = 0.10h_c$ and $d = 0.70h_c$ (Verseghy et al., 1993). In addition, following Brutsaert (1979) and Garrat and Hicks (1973), the relation of z_{0m} and z_{0h} is assumed as follows

$$z_{0h} = z_{0m}/2.0 \quad \text{(forest)} \tag{9}$$

$$z_{0h} = z_{0m}/7.0 \quad \text{(crops)} \tag{10}$$

$$z_{0h} = z_{0m}/12.0 \quad \text{(grass)} \tag{11}$$

The atmospheric stability correction factor, η, is taken as

$$\eta = 5(z-d)g(T_0 - T_a)/T_a u_a^2 \tag{12}$$

where T_a is the air temperature at the reference height, g is the gravitational acceleration. Practically, T_0 can be thought of as an effective aerodynamic turbulence surface temperature calculated as a weighted average of soil and canopy temperature (De Ridder and Schayes, 1997). Or it can be derived from energy balance equations with first- or second-order Taylor approximation for outgoing longwave radiation and saturation vapor pressure terms (Lhomme, 1992; Gao, 1995). In this study, Gao's scheme is adopted.

2.2.2. Canopy resistance

Canopy resistance is calculated as a summation of the leaf stomatal resistance of individual leaves, which is assumed to contribute in parallel. Generally, the leaf stomatal resistances of dense, green and unstressed canopies are all low, ranging from 50 to 200 s m^{-1} (Verseghy et al., 1993). In nature, various environmental factors, such as incoming solar radiation, air water vapor deficit, soil moisture deficit in the rooting zone, and canopy temperature, modulate the leaf stomatal resistance. Based on the scheme proposed by Jarvis (1976), the canopy resistance is parameterized as a multiple response of leaf stomatal resistance to the environmental factors

$$r_c = \frac{r_{smin}}{LAI} f_1(R_s^{\downarrow}) f_2(D_0) f_3(T_0) f_4(\theta_2) \tag{13}$$

where r_{smin} is the minimum stomatal resistance, LAI is the leaf area index. For simplicity, the quantities $f_1(\cdot)$, $f_2(\cdot)$, $f_3(\cdot)$ and $f_4(\cdot)$ are taken as the functions of the incoming shortwave solar radiation $R_s^{\downarrow}$, air water vapor deficit D_0, temperature T_0, and soil moisture θ_2. In this paper, the following simple relations are used (Stewart, 1988; Irannejad and Shao, 1998)

$$f_1(R_s^{\downarrow}) = 1 - \exp(-R_s^{\downarrow}/500) \tag{14}$$

$$f_2(D_0) = 1 - 0.0238 D_0 \tag{15}$$

$$f_3(T_0) = 1 - 1.6 \times 10^{-3}(298 - T_0) \tag{16}$$

$$f_4(\theta_2) = \begin{cases} 1, & \theta_2 \geq \theta_c \\ \dfrac{\theta_2 - \theta_w}{\theta_c - \theta_w}, & \theta_c < \theta_2 < \theta_w \\ 0, & \theta_2 \leq \theta_w \end{cases} \tag{17}$$

where θ_c is the moisture content below which transpiration is stressed by soil moisture, taken as $0.75\theta_{sat}$ (e.g. in Irannejad and Shao, 1998). θ_w is the plant permanent wilting point. In this study, the saturated soil moisture θ_{sat} is set as 0.4 cm^3 cm^{-3} and the wilting point as 0.1 cm^3 cm^{-3} for sandy loam in the North China Plain.

2.2.3. Soil resistance

Soil resistance describes the impedance of soil pores to the exchange of water vapor between the soil surface and the immediately overlying air, which is usually related to the near surface soil moisture content. The relation used in the present study is (Sellers et al., 1992)

$$r_s = \exp(8.206 - 4.255\zeta) \tag{18}$$

where ζ is the fraction of surface layer (0.1 m) soil moisture (θ_1), expressed as a fraction of the saturated moisture content.

2.2.4. Bulk boundary-layer resistance of a canopy and aerodynamic resistance between soil surface and canopy air space

It is assumed that heat and water vapor are exchanged by molecular diffusion through a laminar layer around the leaves, and that wind speed attenuates exponentially inside the canopy. The bulk boundary-layer resistance of a canopy is estimated by integrating the leaf boundary-layer resistance over the canopy height with uniform leaf area density (Choudhury and Monteith, 1988)

$$r_{ac} = \frac{\alpha_w}{4\alpha_0[1 - \exp(-\alpha_w/2)]} \frac{(l/u_h)^{1/2}}{LAI} \tag{19}$$

where l is a characteristic length scale for an average leaf width, u_h is the wind speed at canopy height, α_w is the wind extinction coefficient in the canopy (taken as 2.5), α_0 is a coefficient taken as 0.005 $ms^{-1/2}$.

Aerodynamic resistance between the soil surface and canopy air space (source height) is affected by many factors, making it difficult to characterize. Choudhury and Monteith (1988) defined it as the integral of the reciprocal of eddy diffusivity from soil roughness to source height. Considering free convective conditions, Norman et al. (1995) and Kustas and Norman (1999) introduced a simplified equation,

which is expressed as

$$r_{as} = \frac{1}{a + bu_s} \tag{20}$$

where a and b are constants ($a = 0.004$ m s^{-1}, $b = 0.012$), u_s is the wind speed at a height above the soil surface where the effect of soil surface roughness is minimal, typically 0.05–0.2 m. In this paper, wind speed at 0.2 m is used and calculated from the assumed exponential extinction of wind speed.

2.3. Radiative transfer

2.3.1. Shortwave radiation

The daily variation of downward solar radiation flux, $R_s^{\downarrow}$, is described as the sum of trigonometric functions with four harmonics (Kondo and Xu, 1997)

$$R_s^{\downarrow} = R_{sm}^{\downarrow}\left\{1 + \sum_{n=1}^{4} A_n \cos(n\omega t)\right\} \tag{21}$$

where $A_1 = -1.503$, $A_2 = 0.584$, $A_3 = -0.058$ and $A_4 = -0.023$, ω is the angular velocity of the diurnal cycle, t is time in seconds. The daily mean downward solar radiation flux, $R_{sm}^{\downarrow}$, is calculated from sunshine duration (Kondo and Xu, 1997)

$$\frac{R_{sm}^{\downarrow}}{R_{sm0}^{\downarrow}} = \begin{cases} a_s + b_s \dfrac{N}{N_0}, & 0 < \dfrac{N}{N_0} \le 1 \\ c_s, & \dfrac{N}{N_0} = 0 \end{cases} \tag{22}$$

where

$$a_s = 0.179 + 0.32(1 - P_a/1000) \tag{23}$$

$$b_s = 0.55 \tag{24}$$

$$c_s = 0.114 + 0.32(1 - P_a/1000) \tag{25}$$

Here, N and N_0 are the observed and possible sunshine durations in hours, respectively, $R_{sm0}^{\downarrow}$ is the daily mean downward solar radiation at the top of the atmosphere and P_a is the atmospheric pressure.

2.3.2. Longwave radiation

The downward longwave radiation is estimated as (Kondo and Xu, 1997)

$$R_l^{\downarrow} = \sigma T_a^4 \left[1 - \left(1 - \frac{R_{lf}^{\downarrow}}{\sigma T_a^4}\right) C\right] \tag{26}$$

where σ is the Stefan–Boltzmann constant, C is related to the fraction of sunshine hours and expressed as

$$C = \begin{cases} 0.826\left(\dfrac{N}{N_0}\right)^3 - 1.234\left(\dfrac{N}{N_0}\right)^2 + 1.135\left(\dfrac{N}{N_0}\right) + 0.29 & 0 < N/N_0 \le 1 \\ 0.2235 & N/N_0 = 0 \end{cases} \tag{27}$$

The quantity $R_{lf}^{\downarrow}$ is the downward longwave radiation under clear sky, expressed as (Zuo et al., 1991)

$$R_{lf}^{\downarrow} = (0.614 + 0.057\sqrt{e_a})\sigma T_a^4 \tag{28}$$

where e_a is the atmospheric vapor pressure at the reference height.

2.3.3. Absorbed radiation of canopy and soil surface

The net radiation above the canopy top is calculated as

$$R_n = R_s^{\downarrow}(1 - \alpha) + R_l^{\downarrow} - \varepsilon\sigma T_0^4 \tag{29}$$

where α is the surface albedo, ε is the surface emissivity, set as 0.97 for vegetation canopy.

The net radiations absorbed by canopy, R_{nc}, and soil surface, R_{ns}, are partitioned with an exponential attenuation, expressed as (Kustas and Norman, 1999)

$$\begin{aligned} R_{nc} &= R_n - R_{ns} \\ &= R_n[1 - \exp(-K\mathrm{LAI}/\sqrt{2\cos\Theta_s})] \end{aligned} \tag{30}$$

where Θ_s is the solar zenith angle and K is the extinction coefficient of net radiation, which is usually in the limit of 0.3–0.6 (Ross, 1975). In this study, K is taken as 0.5.

As a component of soil surface energy balance, the soil heat flux affected by incident radiation and soil moisture condition is observed to be linearly related to the net radiation of soil surface for several hours around noon. Choudhury et al. (1987) took it as $0.35R_{ns}$ under a growing wheat canopy.

By regressing field data of maize in the North China Plain, a relation between G/R_n and LAI is obtained as (Mo et al., 2002)

$$G/R_n = 0.183 \exp(-0.299\mathrm{LAI}) \quad (31)$$

2.4. Soil water, surface runoff and interception

2.4.1. Soil moisture

The dynamics of soil moisture is described with a three-layer scheme, in which the first layer acts as a significant source of soil evaporation, the second as the source of root uptake for canopy transpiration and the third layer as the drainage layer. The governing equations are expressed as follows

$$\frac{\partial \theta_1}{\partial t} = \frac{1}{L_1}[P' - Q_{12} - E_s] \quad (32)$$

$$\frac{\partial \theta_2}{\partial t} = \frac{1}{L_2}[Q_{12} - Q_{23} - E_c] \quad (33)$$

$$\frac{\partial \theta_3}{\partial t} = \frac{1}{L_3}[Q_{23} - Q_3] \quad (34)$$

where θ_i $(i = 1, ..., 3)$ is the soil moisture in the soil layer i with thickness L_i. P' is the residual amount of precipitation minus canopy interception and overland runoff. $Q_{i,i+1}$ $(i = 1, 2)$ is the flow between the i and $i + 1$ layers, Q_3 is the gravitational drainage from the bottom layer. Fluxes $Q_{i,i+1}$ and Q_3 are estimated as (Sellers et al., 1986)

$$Q_{i,i+1} = \frac{L_i K_{w,i} + L_{i+1} K_{w,i+1}}{L_i + L_{i+1}} \left(2\frac{\psi_i - \psi_{i+1}}{L_i + L_{i+1}} + 1\right) \quad (35)$$

$$Q_3 = K_{w,3} \sin(x) \quad (36)$$

where $K_{w,i}$ $(i = 1, ..., 3)$ is the hydraulic conductivity of the ith layer, ψ_i is the water potential of layer i, x is the slope angle. $K_{w,i}$ and ψ_i are estimated by the relationship of Clapp and Hornberger (1978) with parameters (saturated conductivity K_{wsat}, air entry value ψ_s and constant B) for sand loam given by Sellers et al. (1996).

2.4.2. Interception

It is assumed that the rain falls vertically and the interception of rain by the canopy can be treated the same way as direct light incident at zero zenith angles (De Ridder and Schayes, 1997). According to this assumption, the interception is calculated with

$$W_r = \delta P \quad (37)$$

where W_r is the interception of rainfall, P is the precipitation above the canopy, δ is the fraction of vegetation. Whenever the canopy's water holding capacity $(W_r^{max}(\mathrm{mm}) = 0.2\mathrm{LAI})$ is exceeded, the excess water drips from leaves to the ground surface. δ is expressed as follows

$$\delta = 1 - \exp(-0.5\mathrm{LAI}) \quad (38)$$

The wetted fraction of the canopy is calculated by the following method (Noilhan and Planton, 1989)

$$W_{fr} = \left(\frac{W_r}{W_r^{max}}\right)^{2/3} \quad (39)$$

2.4.3. Surface runoff

The magnitude and the timing of the overland runoff are affected by many factors, being mainly rainfall intensity, soil moisture condition, and land use. The overland runoff is simply treated as (Choudhury and Digirolamo, 1998)

$$Q_f = p'2/(p' + \mu) \quad (40)$$

where Q_f is the surface runoff, μ is the soil moisture deficit in the root zone, expressed as

$$\mu = (L_1 + L_2)\theta_{cri} - (L_1\theta_1 + L_2\theta_2) \quad (41)$$

where θ_{cri} is the critical soil moisture in the root zone over which the runoff occurs as saturation excess, and under which as infiltration excess. L_1 and L_2 are defined in Eqs. (32)–(34).

3. Study area and data preparation

3.1. Description of the study area

The Lushi basin is a sub-basin of a tributary in the middle reach of the Yellow River as shown in Fig. 1. The basin is a mountainous region with an area about 4423 km^2 and altitude range of 550–2500 m from east to west. The data recorded in 10 rainfall gauges and 1 meteorological station are available over the basin from 1983 to 1997.

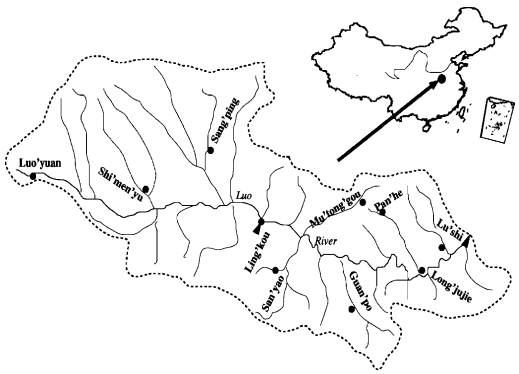

Fig. 1. The Lushi basin, China.

Average annual precipitation is approximately 650 mm. The vegetation types and land use are digitized from the 1:1,000,000 scale land use map (Wu, 1992) and re-classified into six types, namely arid farmland, broadleaf forest, coniferous forest, dwarf shrub, grass and irrigated farmland (Fig. 2). The fractions of the relevant land use types are 22, 14, 16, 9, 36 and 2%, respectively.

3.2. Data preparation

The raw data for the simulation falls into three main categories: (1) topography; (2) time-series of meteorological and hydrological data and (3) land surface characterization, described briefly as follows.

3.2.1. Topography

The topography of the Lushi basin is described with the digital elevation model (DEM) data. In this study, the topographical data ($30'' \times 30''$) (Fig. 3) were obtained from the US Geological Survey database.

3.2.2. Meteorology

Based on the DEM, the key meteorological variables (daily mean, maximum and minimum air temperature, air water vapor pressure, wind velocity and precipitation) are topographically corrected with the empirical relationships presented by Fu and Lu (1990)

$$T_a = -0.502Z_{100} + T_{a,obs} \quad (42)$$

$$e_a = e_{a,obs} \exp(-0.0257Z_{100}) \quad (43)$$

$$u_a = u_{a,obs}\{3.6 - 2.6\exp[-0.0569(Z_{100} - 0.6)]\} \quad (44)$$

$$P = P_{obs}(1 + 0.043Z_{100}) \quad (45)$$

where Z_{100} is the altitude in one hundred meters. The quantities $T_{a,obs}$, $e_{a,obs}$ and $u_{a,obs}$ are the air temperature, air water vapor pressure and wind speed recordings in the meteorological station, respectively. P_{obs} is the recorded precipitation. The spatial pattern of precipitation is usually highly inhomogeneous, whereas the temperature is mainly affected by topographical altitude at the basin scale. The precipitation measurements at 10 sites are interpolated over the whole basin with the inverse distance square method (Ashraf et al., 1997).

3.2.3. Land surface characterization

The model characterizes the land surface at the same spatial scale as the DEM, including the soil and vegetation properties. In each grid cell, the land surface is composed of canopy and underneath soil surface for different vegetation types. For the soil

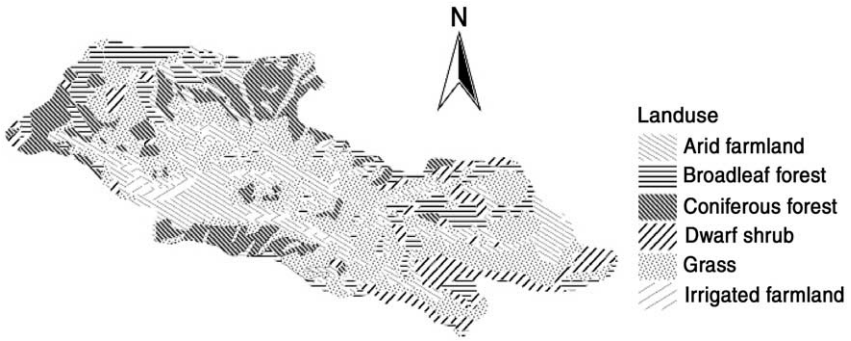

Fig. 2. The land use/cover over the Lushi basin.

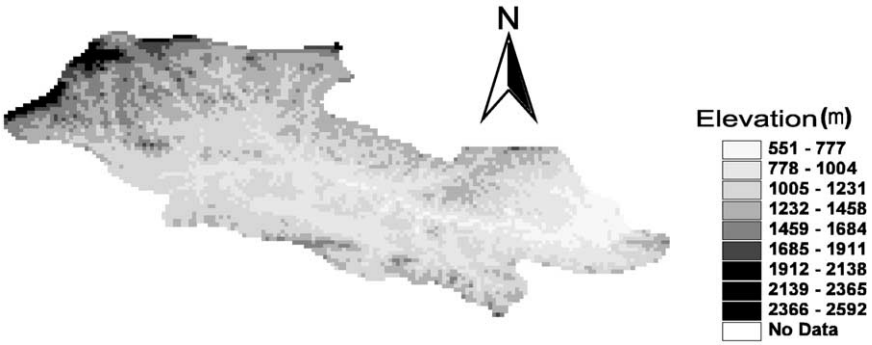

Fig. 3. The digital elevation model (DEM) of the Lushi basin (USGS $30'' \times 30''$ global topographical database).

properties, however, only the values of parameters for sand loam are used, since the basin is composed largely of sand loam and the spatial distribution of soil texture is not available at the moment. The vegetation variables and parameters used in this study are LAI, canopy height, minimum leaf stomatal resistance, albedo and extinction coefficient of net radiation. The extinction coefficient of net radiation is taken as 0.5 for all the vegetation types, other vegetation parameters and the values of the maximum of NDVI are shown in Table 1.

For the farmland, it is assumed that the dominant crop types are winter wheat and summer maize, which are the prevailing cultivars in the basin. Based on our measured data in the North China Plain which is close to the Lushi basin, canopy height and LAI are fitted as logistic curves, relating to cumulative days since planting date (DSP) or days since recovering green in spring (DSR). The relations for maize are as follows

$$h_c = h_{c,max}/(1 + \exp(4.052 - 0.124\mathrm{DSP})) \quad (46)$$

$$\mathrm{LAI} = 4.8/\{1 + \exp[-0.797 - 0.105(\mathrm{DSP} - 37) + 0.00222(\mathrm{DSP} - 37)^2]\} \quad (47)$$

For winter wheat

$$h_c = h_{c,max}0.812/(1 + \exp(1.054 - 0.054\mathrm{DSR})) \quad (48)$$

$$\mathrm{LAI} = 11.25/\{1 + \exp[0.122 + 0.0067(\mathrm{DSR} - 51.5) + 0.000787(\mathrm{DSR} - 51.5)^2]\} \quad (49)$$

where h_c, $h_{c,max}$ are the canopy height and its maximum, respectively, DSR starts from the day while mean air temperature is over 3 °C).

Leaf area index and canopy height of natural vegetations can also be estimated from their phenological stages. For trees, including deciduous

Table 1
Biophysical parameters adopted in the model

No.	Vegetation type	Ratio (%)	α	r_{smin} (s m^{-1})	LAI_{max}	LAI_{min}	h_{cmax} (m)	$NDVI_{max}$
1	Arid farmland	22	0.2	100	6	0.1	0.8	0.674
2	Broadleaf forest	14	0.16	130	6	0.5	20	0.721
3	Coniferous forest	16	0.14	150	5	3	15	0.689
4	Dwarf shrub	9	0.16	120	4	0.5	1.5	0.674
5	Grass	36	0.20	110	4	0.1	0.8	0.611
6	Irrigated farmland	2	0.18	100	6	0.1	0.8	0.674

Source: α and r_{smin} are from Wang and Takahashi (1999), Kergoat (1998) and our field experiments; LAI_{max}, LAI_{min}, h_{cmax} and $NDVI_{max}$ are from Sellers et al. (1996).

broadleaf forest, dwarf shrub and coniferous forest, a growth index, β, is defined to account for the seasonal variations of LAI. The index β has a value of 1 during periods when the vegetation is mature and/or fully leafed and a value of 0 during dormant and leafless periods; the transition between the two is taken to be linear (Verseghy et al., 1993). Canopy heights of trees are set as fixed values and LAI is computed by

$$\mathrm{LAI} = \mathrm{LAI}_{\min} + \beta(\mathrm{LAI}_{\max} - \mathrm{LAI}_{\min}) \quad (50)$$

For grass, LAI and canopy height are expressed as

$$\mathrm{LAI} = \frac{h_c}{h_{c,\max}}[\mathrm{LAI}_{\min} + \beta(\mathrm{LAI}_{\max} - \mathrm{LAI}_{\min})] \quad (51)$$

and

$$h_c = \beta(h_{c,\max} - h_{c,\min}) + h_{c,\min} \quad (52)$$

where $\mathrm{LAI}_{\max}$ and $\mathrm{LAI}_{\min}$ are the maximum and minimum of LAI, respectively, $h_{c,\min}$ is the minimum of h_c.

As an alternative, spectral vegetation indices from satellite-based spectral observation, such as NDVI, or simple ratio ($\mathrm{SR} = (1 + \mathrm{NDVI})/(1 - \mathrm{NDVI})$, are widely used to extract vegetation biophysical parameters of which LAI is the most important. The use of monthly vegetation index is a good way to take into account the phenological development of the LAI, as well as the effects of prolonged water stresses that reduce the LAI (Maisongrande et al., 1995). In this study, monthly maximum composite 1-km resolution NDVI dataset obtained from NOAA-AVHRR (National Oceanic and Atmospheric Administration-Advanced very High Resolution Radiometer) in 1992, 1995 and 1996 were used to estimate LAI. The simple relationships between LAI and NDVI were taken from SiB2 (Sellers et al., 1996). For evenly distributed vegetation, such as grass and crops

$$\mathrm{LAI} = \mathrm{LAI}_{\max}\frac{\log(1 - \mathrm{FPAR})}{\log(1 - \mathrm{FPAR}_{\max})} \quad (53)$$

For clustered vegetation, such as coniferous trees and shrubs

$$\mathrm{LAI} = \frac{\mathrm{LAI}_{\max}\mathrm{FPAR}}{\mathrm{FPAR}_{\max}} \quad (54)$$

where FPAR is the fraction of photosynthetically active radiation absorbed by the canopy, calculated as

$$\mathrm{FPAR} = \frac{(\mathrm{SR} - \mathrm{SR}_{\min})(\mathrm{FPAR}_{\max} - \mathrm{FPAR}_{\min})}{\mathrm{SR}_{\max} - \mathrm{SR}_{\min}} \quad (55)$$

where $\mathrm{FPAR}_{\max}$ and $\mathrm{FPAR}_{\min}$ are taken as 0.950 and 0.001, respectively. $\mathrm{SR}_{\max}$ and $\mathrm{SR}_{\min}$ are SR values corresponding to 98 and 5% of NDVI population, respectively. Fig. 4 shows the NDVI-derived LAI averaged for each vegetation type in the basin. As shown in Fig. 4, LAI was higher than 1 for most

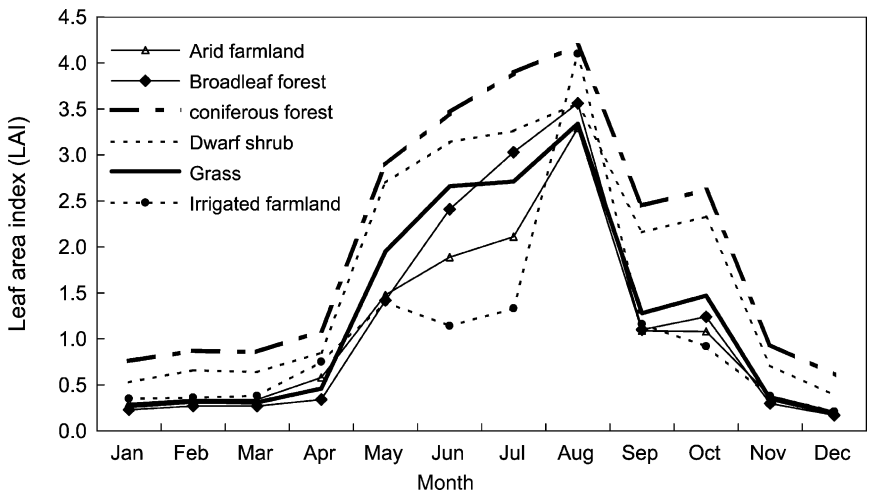

Fig. 4. Monthly courses of leaf area index (LAI) of the vegetation types over the Lushi basin, retrieved from the monthly maximum composite NDVI in 1996.

vegetation types from May to October with the maximum LAI occurring in August for all six vegetation types, which represented the active period of growth and transpiration in the vegetations. Due to maturity and harvest of wheat, LAI fell down in June over agricultural field.

3.3. Initial model state

The meteorological variables were daily mean temperature, maximum and minimum temperature, vapor pressure, wind speed and sunshine duration in hours. The diurnal variations of air temperature and global radiation were fitted by two-harmonic waves (Kondo and Xu, 1997), and LAI was also interpolated into daily values. As the initial condition of soil moisture was not available, the spatial pattern of soil moisture after one-year run was used as the initial state. Then another one-year run was done to warm up the model simulation. In order to check the effects of warming up on the simulation results, two and three years warming up runs were also carried out, respectively. It was shown that the differences of simulated annual evapotranspiration between one-year run and two or more years warming up run were less than 2 mm.

The depths of the three soil layers were set as 0.1, 1.9 and 2 m, respectively, assuming that the vegetation rooting depth is up to 2 m and the roots are limited to draw water directly from this volume. It is reported that the average maximum rooting depth was about 7 m for trees and 2.6 m for herbaceous plants (Canadell et al., 1996). Some trees have active roots over great depths, here we assumed that the active root zone in the basin is within 2 m depth.

4. Result analysis

4.1. Yearly evapotranspiration values simulated with LAI retrieved from NDVI in three different years and from the phenological method

Lacking of long-term datasets of NDVI, the NDVI dataset for 1996 was used as an alternative for other years in this study. To test the representativeness of the 1996 NDVI-derived LAI for other years, the annual evapotranspiration (E_{Ta}) (summation of canopy transpiration, evaporation and soil evaporation) is calculated from 1984 to 1997 with LAI derived by 1996 NDVI and the phenological method cell by cell, respectively. The average difference of simulated annual E_{Ta} is 42 mm or 7% for 14 years. As the spatial pattern of vegetation characteristics shows a good relation with the remotely sensed NDVI, the simulated E_{Ta} with NDVI is often considered more reliable than that with the phenological method. Since the LAI time-series of vegetation in the basin might fluctuate to a greater or lesser extent in each year, we also compared annual E_{Ta}, E_{ca} (transpiration) and E_{sa} (soil evaporation) values simulated with 1992, 1995 and 1996 NDVI data to justify the yearly variations of annual E_{Ta}, E_{sa} and E_{ca} caused by yearly NDVI variation (Fig. 5). The results show that the differences of annual simulated E_{Ta}, E_{sa} and E_{ca} by using LAI derived from 1992 NDVI and 1996 NDVI are within 10 mm when the precipitation amounts in these two years are similar. Simulated E_{Ta}, E_{ca} and E_{sa} by using LAI derived from 1995 NDVI are slightly different from those derived from 1996 NDVI data, where the maximum and mean absolute (relative) differences of E_{Ta} are 30 mm (5%) and 17 mm (3%), respectively. This suggests that the influence of annual variation of LAI occurring at NOAA-AVHRR NDVI resolution

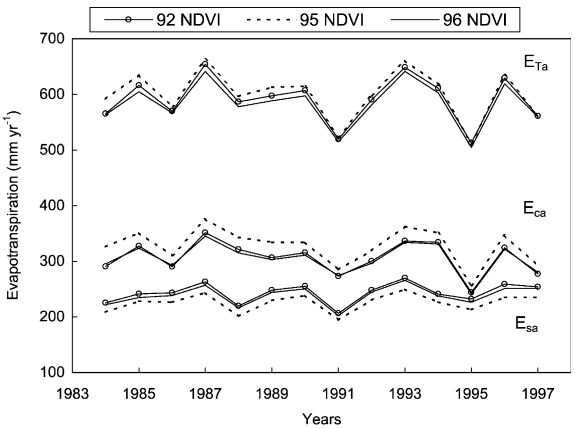

Fig. 5. Simulated annual evapotranspiration (E_{Ta}), transpiration (E_{ca}) and soil evaporation (E_{sa}) with 1992, 1995 and 1996 monthly maximum composite NDVI from 1984 to 1997.

Table 2
Water balance components for the Lushi basin

Year	Precipitation (mm)	Storage change (mm)	Modeled annual E_{Ta} (mm)	Measured discharge (mm)	The relative error of annual E_{Ta} (%)
84	977	14	567	350	7.3
85	780	0	609	240	−12.8
86	546	−54	571	33	−0.7
87	823	8	645	140	4.4
88	768	44	581	189	−7.9
89	783	−20	592	167	7.1
90	619	−66	601	103	−3.7
91	569	12	518	52	−2.6
92	844	66	585	160	4.8
93	738	−38	645	67	9.5
94	701	−18	607	117	−0.8
95	504	2	508	28	−7.3
96	801	66	623	165	−8.3
97	460	−116	563	35	−5.3
Mean	708		587	143	
σ/Mean	0.21		0.07	0.66	

pixel is acceptable for the simulation purpose of annual E_{Ta}. Thus in the next step the yearly evolution of LAI derived from 1996 NDVI is used for the whole study period.

4.2. Annual water balance

The annual water balance components are listed in Table 2 from 1984 to 1997 in which the mean annual precipitation, discharge and simulated annual evapotranspiration (E_{Ta}) are 708, 143 and 587 mm, respectively. The standard deviation (σ) of simulated E_{Ta} over all the simulated years is 40 mm, much less than that of precipitation ($\sigma =$ 148 mm) and discharge ($\sigma = 87$ mm). As a component of water balance, the modeled annual water storage change (ΔS) in the root zone oscillated in a range of −116 to 66 mm. The coefficient of interannual variation of evapotranspiration in the Lushi basin is 7% ($\sigma/\bar{x}$), while that for precipitation, discharge and net radiation (not shown in the table) are, respectively, 20, 66 and 10%. Due to the limitation to get enough groundwater data, the above results are based on model assumption that the change of ground water storage is negligible over annual cycle. For the annually simulated ($y_{i,sim}$, taken as $E_{Ta} + \Delta S$) and measured ($y_{i,obs}$, taken as $P_{obs} - Q_{obs}$) values (Fig. 6), the root mean square difference (RMSD) of model prediction to observation, which is defined as

$$\mathrm{RMSD} = \sqrt{\frac{1}{n}\sum_{i}(y_{i,\mathrm{sim}} - y_{i,\mathrm{obs}})^2}$$

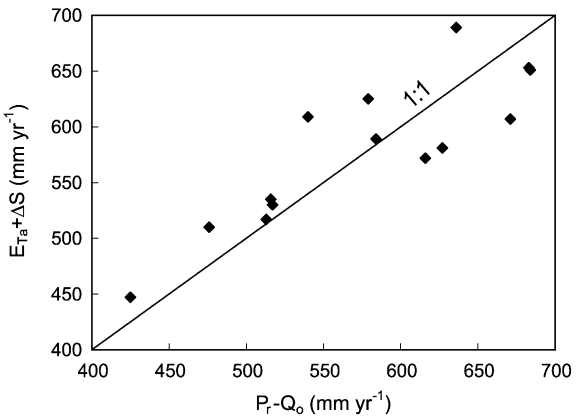

Fig. 6. Comparison of the simulated annual E_{Ta} plus soil moisture storage change (ΔS) in the root zone with the precipitation (P_r) minus the discharge depth (Q_o) from 1984 to 1997.

is 39 mm, and the mean absolute percent difference (MAPD), which is defined as

$$\mathrm{MAPD} = 100\frac{\sum_i |y_{i,\mathrm{sim}} - y_{i,\mathrm{obs}}|}{\sum_i y_{i,\mathrm{obs}}}$$

is 6%.

4.3. Spatial patterns of annual evapotranspiration, transpiration and soil evaporation

Fig. 7(a)–(e) shows the spatial patterns of annual precipitation, evapotranspiration, canopy transpiration, soil evaporation and LAI (in August) in 1996. Since vegetation canopy is fully leafed and LAI always reaches its maximum in August, we use the LAI in August to represent the vegetation condition in the basin. It is shown that there is significant heterogeneity at the basin scale for these components. The annual precipitation shows a pattern clearly similar to the basin topography (Fig. 3), where there are heavier rainfalls in the mountains than in the valleys. Considerable inhomogeneities of vegetation densities also exist, with dense vegetation with high LAI in the mountainous regions and sparse vegetation with low LAI in the central and outlet areas of the basin. As a consequence, higher E_{Ta} and transpiration

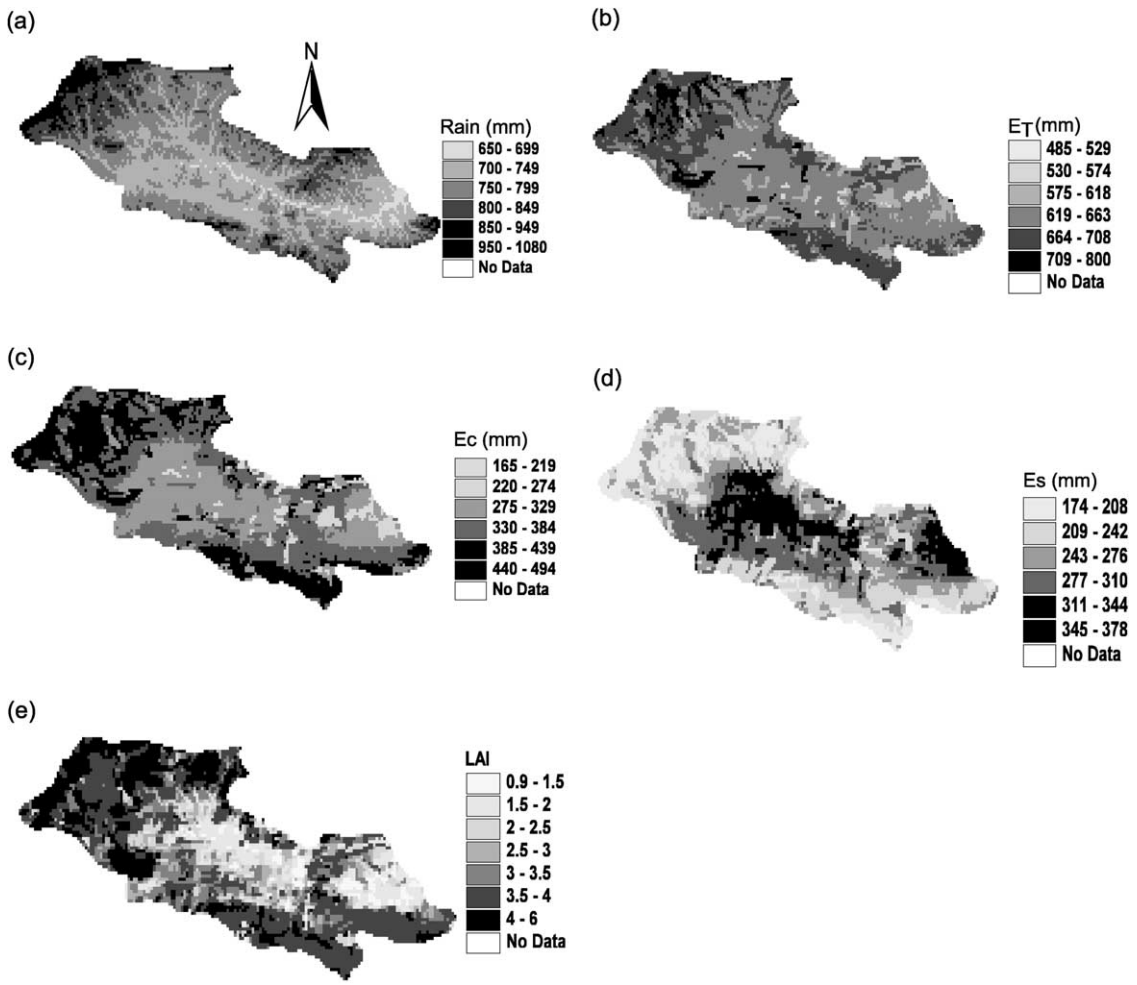

Fig. 7. The spatial patterns of annual precipitation (a), evapotranspiration (b), canopy transpiration (c), soil evaporation (d) and LAI in August (e) in 1996 over the basin.

Table 3
Net radiation (mm equivalent evaporation), evapotranspiration and its components for vegetation types (mm)

Vegetation type	R_n	E_{Ta}	E_{ca}	E_{sa}	E_{ia}	E_{ca}/E_{Ta} (%)
Arid farmland	1520	636	317	282	36	50
Broadleaf forest	1685	567	255	270	41	45
Coniferous forest	1709	593	321	206	64	54
Dwarf shrub	1615	640	369	214	55	58
Grass	1511	635	338	261	42	53
Irrigated crop	1525	699	363	302	33	52
Average	1594	628	327	256	45	
Standard deviation	88	45	41	38	12	
Coefficient of variation	0.06	0.07	0.13	0.15	0.26	

occur in the high precipitation and dense vegetation areas and vice versa. It is also shown that lower evapotranspiration with high fraction of soil evaporation occurs in the arid farmland in the middle and outlet areas of the basin (Fig. 2). Fig. 7 also shows that the E_{Ta} pattern does not fully match the vegetation pattern that is dependent on the combination of vegetation and climate (Silberstein and Sivapalan, 1995). Over the whole basin, significant variations of E_{Ta} values exist among grid cells with different vegetation types, ranging from 580 to 720 mm yr^{-1} in arid farmland and grassland, 510–660 mm yr^{-1} in broadleaf forest and 550–650 mm yr^{-1} in coniferous forest, respectively.

From Table 3, it is seen that the highest predicted E_{Ta} occurred in irrigated fields with an average of 699 mm yr^{-1} due to irrigation water supply (set as 150 mm yr^{-1} and added to fields with 50 mm each time). The two lowest simulated E_{Ta} amounts occurred in broadleaf forest and coniferous forest with 567 and 593 mm yr^{-1}, respectively. This is related to the fact that the minimum leaf stomatal resistance is an important parameter that determines the transpiration rates. Non-optimal air temperature and vapor pressure in trees will increase stomatal resistance, leading to reduction of canopy transpiration rate. The larger stomatal resistance in tree canopy leaves also explains why E_{Ta} is smaller in woody lands than the herbaceous land. Since there are more grids with low LAI in the broadleaf forest, its averaged E_{Ta} is lower than those from other vegetation types. Over the whole basin, the fractions of annual transpiration to evapotranspiration are within a range of 45–58%. The coefficient of variation of E_{Ta} is lower compared with the coefficients of its components (E_{sa}, E_{ca} and E_{ia}) with that of the canopy E_{ia} being highest. Except for broadleaf forest, annual transpiration for each vegetation type is larger than the soil evaporation. The simulated annual evapotranspiration averaged over each vegetation type for the whole basin in 1996 was 628 mm, with the transpiration 327 mm, soil evaporation 256 mm and interception evaporation 45 mm.

4.4. Seasonal variation of the evapotranspiration

Fig. 8 presents the evolution of total monthly evapotranspiration (Here in after in this

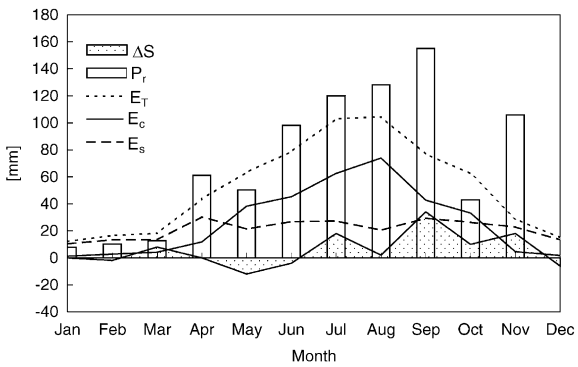

Fig. 8. Monthly course of evapotranspiration (E_T), canopy transpiration (E_c), soil evaporation (E_s), precipitation (P_r) and water storage change in the root zone (Δs) in 1996.

section denoted as E_{Tm}), transpiration, soil evaporation, precipitation and soil storage change in the basin in 1996. The seasonal variation pattern of E_{Tm} was correspondent to the incoming shortwave radiation flux (not shown in the figure) and vegetation canopy leaf growth phenological stages, as well as rainy season. It showed that the highest E_{Tm} occurred in the period of July to August with 104 mm month^{-1}, relating to adequate precipitation and fully developed vegetation canopy, as well as high downward radiation fluxes. This period coincided with the rainy season while the summer monsoon was prevailing. Although annually the evaporation from the soil surface was less than the canopy transpiration, the monthly soil evaporation was an important component of E_{Tm} in all the months. The monthly evolution of soil evaporation showed that the highest rate was in spring and autumn when canopy leaves were growing and senescing, respectively, resulting from intensive atmosphere evaporative demand in these seasons. It also showed that canopy transpiration exceeded soil evaporation only in summer when the vegetation canopy had fully grown.

Fig. 9 shows the evolution of simulated monthly evapotranspiration for each vegetation type. The E_{Tm} from irrigated farmland was higher than that from other vegetation types all the year although the irrigating water was put into the field only in spring while wheat was growing. The E_{Tm} amounts for grass and arid farmland were similar and about 10 mm month^{-1} higher than that for the forests in summer. The high evapotranspiration rates with

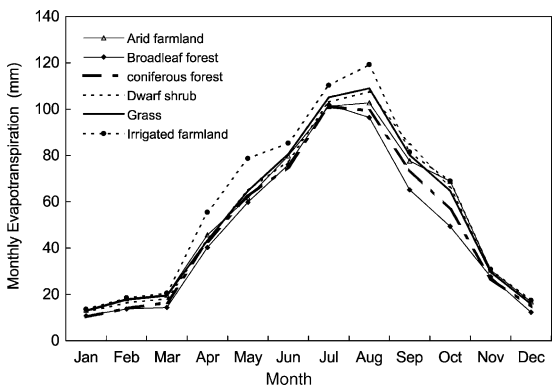

Fig. 9. Monthly course of the averaged evapotranspiration over the six vegetation types in 1996.

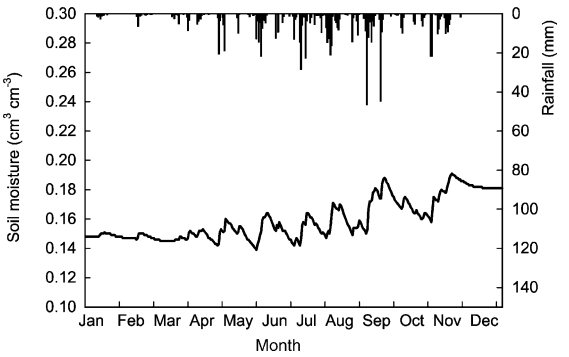

Fig. 10. Daily evolution of the averaged soil moisture in root zone and rainfall in 1996.

100 mm month^{-1} or more for all the vegetation types only held through July and August, after which the evapotranspiration rates decreased rapidly for all the vegetation types.

The average simulated soil moisture in the root zone increased with rainfall events, and decreased afterwards (Fig. 10). The simulated highest soil moisture was 0.19 cm^3 cm^{-3} in the early winter and the highest daily evapotranspiration is about 5 mm d^{-1}.

5. Parameters sensitivity analysis

Shown in Fig. 11(a)–(f) are the sensitivities of six principal parameters in the model, namely the canopy extinction coefficient of net radiation (K), the minimum stomatal resistance (r_{smin}), the depths of top soil layer (L_1) and second layer (L_2), the soil saturated hydraulic conductivity (K_{wsat}), and the critical soil moisture (θ_{cri}) for infiltration (Eqs. (40) and (41)), to the simulated annual evapotranspiration (E_{Ta}), canopy transpiration (E_{ca}) and soil evaporation (E_{sa}). The reference values for K, L_1, L_2, K_{wsat}, and θ_{cri} are set as 0.5, 0.1, 1.9 m, 7×10^{-4} cm s^{-1} and 0.2 cm^{-3} cm^{-3}, respectively. The value for r_{smin} is taken from Table 1 for grass. To clarify the model responses to the possible ranges of parameter values, the model is run only with the grassland, instead of with all the vegetation types in the basin. As shown in Fig. 11(a), E_{Ta} and E_{sa} decreases, whereas E_{ca} enhances as K increases resulting in more net

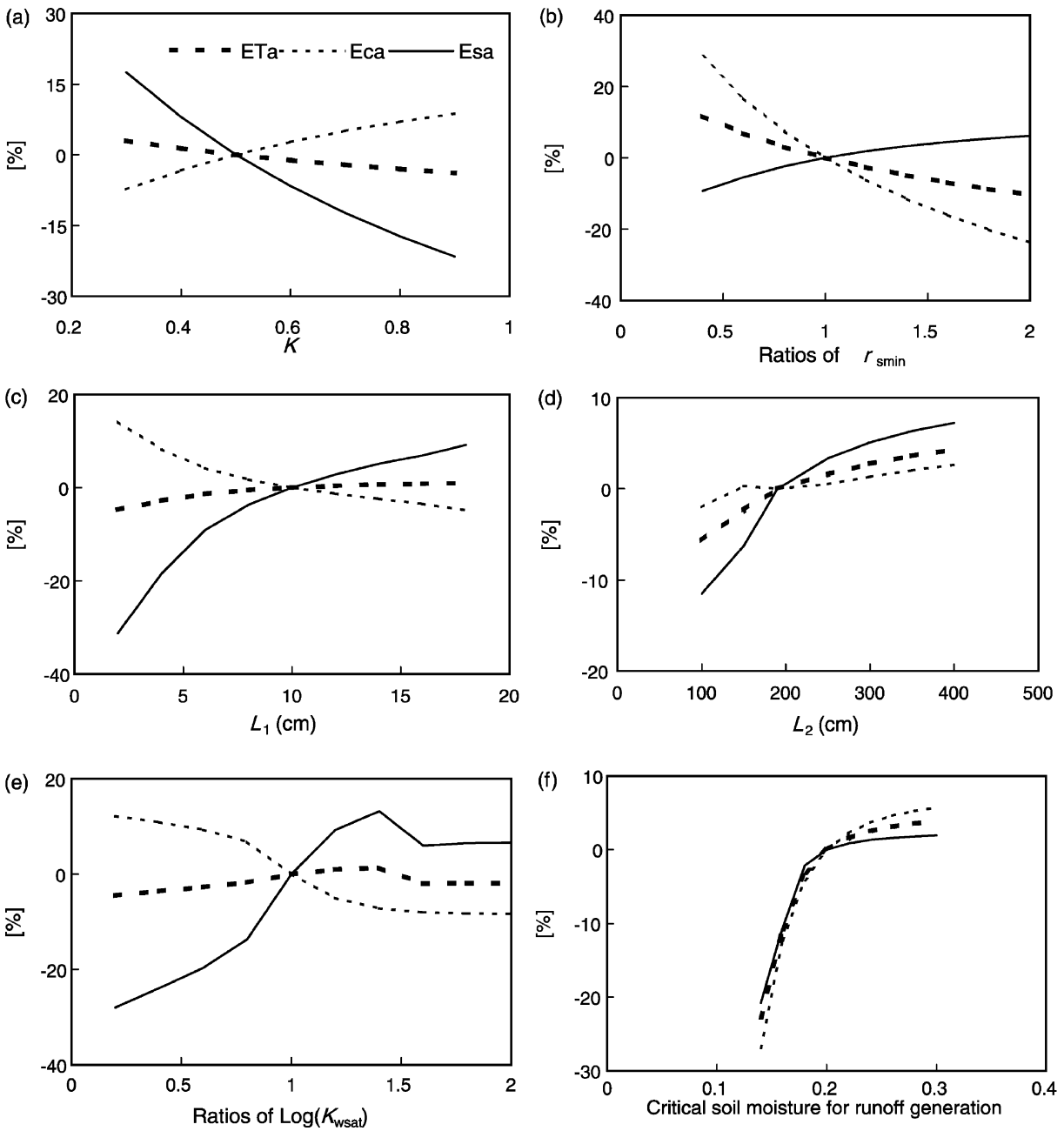

Fig. 11. The sensitivities of annual evapotranspiration (E_{Ta}), transpiration (E_{ca})and soil evaporation (E_{sa})to the canopy extinction coefficient of net radiation (a), the minimum stomatal resistance (b), the depth of top soil layer (c), the depth of the second soil layer (d), the saturated hydraulic conductivity (e) and the critical soil moisture for runoff generation (f).

radiation absorbed by canopy and less by soil surface. As K varies from 0.3 to 0.9, the relative change of E_{sa} to the reference value is from 17 to -21%, while -7 to 9% for E_{ca}, and 3 to -4% for E_{Ta}, respectively. Hence, it can be said that E_{sa} and E_{ca} are very sensitive to K but E_{Ta} is not. Shown in Fig. 11(b), E_{Ta} and E_{ca} are all highly sensitive to the minimum stomatal resistance in the range from 0.4 to 2 times of the reference values. Within this range the relative change of E_{ca} is from 28 to -24%, E_{sa} is from -9 to 6% and E_{Ta} is from 11 to -10%. Therefore bias in the determination of r_{smin} may be the principal cause of model prediction uncertainty. The sensitivity of E_{ca} and E_{sa} to depth of the top soil layer decreases as L_1 increases from 2 to 20 cm. However, the sensitivity of E_{Ta} is less significant (Fig. 11(c)). The depth of layer 2 affects the available moisture for transpiration and capillary rise to layer 1 for evaporation. Fig. 11(d) shows that E_{sa} is relatively more sensitive to the variation of L_2 and the variations of E_{Ta} and E_{ca} are within $\pm 6\%$ from 100 to 400 cm. Since the rainfall offering most water use of canopy, the transpiration does not rely much on the deep soil moisture in summer, but the soil evaporation depends more on the capillary rise from the lower layer in the dry season. While the ratios of $\log(K_{wsat})$ varies from 0.2 to 2, the changes of E_{Ta} are within $\pm 4\%$, whereas E_{ca} and especially E_{sa} show more noticeable responses (Fig. 11(e)). The influences of the critical soil moisture (θ_{cri}) on E_{Ta}, E_{ca} and E_{sa} are significant when θ_{cri} is lower than 0.18 $cm^3\,cm^{-3}$, however, as θ_{cri} varies from 0.18 to 0.3 $cm^3\,cm^{-3}$, the influence is decreasing, especially of E_{Sa} (Fig. 11(f)).

6. Discussions

Comprehensive calibration and uncertainty analysis was not carried out in this study. Although the model could capture the basin temporal pattern of annual evapotranspiration moderately well by comparing with the results derived from the basin water balance, it is still hard to verify the spatial patterns of the simulated results due to the lack of the measured data at the same scale. This may result in significant unavoidable uncertainty in the spatial patterns of the simulated evapotranspiration and its components. Since there was only one meteorological station used in this study, it was impossible to capture spatial heterogeneity of the microclimate over the basin for better model prediction. In addition, the canopy parameters, such as minimum stomatal resistance and, are sensitive to the model prediction, and there are no generally accepted values and information for each vegetation types. Therefore there are still many challenges for distributed modeling. The next step in this work will be to use remotely sensed reflectance and surface temperature with the model to constrain the parameters and reduce the prediction uncertainty.

7. Summary and conclusions

A process-based model is established to simulate the spatial and temporal patterns of evapotranspiration and its components over the Lushi basin. The remotely sensed vegetation index NDVI is used to retrieve the LAI of the vegetation. The precipitation is spatially interpolated over the basin with the inverse distance square method and the meteorological variables are distributed by elevation. The predicted annual evapotranspiration plus soil storage change over the basin is compared with the values calculated by water balance of the basin for 14 years. The RMSD and MAPD between the predicted and the observed are 39 mm and 6%, respectively. Taking 1996 as a study case, the spatial patterns of the annual evapotranspiration and its components are correspondent to the precipitation, vegetation type and leaf area pattern; however, there exists a significant evapotranspiration range in each land cover due to the inhomogeneity of LAI. The annual amount of evapotranspiration was 628 mm with the transpiration 327 mm, soil evaporation 256 mm and canopy interception 45 mm in 1996.

Acknowledgements

The research on which this paper was based was supported by Chinese National Natural Science Foundation (project no. 49771019, 90211007),

Institute of Geographical Sciences and Natural Resources Research (Innovation Knowledge project no. CXIOG-C00-05-01), Knowledge Innovation Project of the Chinese Academy of Sciences KZCX2-310. We would like to thank Prof. K. Beven, Lancaster University for his insightful advice, Dr R.P. Silberstein, CSIRO, Australia, another anonymous reviewer and the editors for their pertinent comments, leading to improvements in the paper.

Appendix A

The surface energy budget can be expressed as follows:

$$R_n = \lambda E + H + G \tag{A1}$$

The bulk aerodynamic expressions for latent and sensible heat fluxes are

$$\lambda E = \frac{\rho C_p}{\gamma} \frac{e_0 - e_a}{r_a} \tag{A2}$$

$$H = \rho C_p \frac{T_0 - T_a}{r_a} \tag{A3}$$

where e_0 and T_0 are the effective water vapor pressure and aerodynamic surface temperature, respectively.

Water vapor deficit D_0 at the aerodynamic surface temperature T_0 can be expressed as

$$D_0 = D + \Delta(T_0 - T_a) - (e_0 - e_a) \tag{A4}$$

By combining Eqs. (A1)–(A4), e_0 and T_0 are eliminated, then

$$D_0 = D + [\Delta(R_n - G) - (\Delta + \gamma)\lambda E] r_a / \rho C_p \tag{A5}$$

To eliminate λE, Eq. (A5) is combined with Eqs. (1) and (2) in the text. Considering that $\lambda E = \lambda E_s + \lambda(E_c + E_i)$ and r_{cw} is r_c weighted by the wetted fraction, an analytical expression for D_0 is derived as follows:

$$\rho C_p D_0 = \frac{\frac{\rho C_p D}{r_a} + \Delta(R_n - G) - A R_{nc} - B(R_{ns} - G)}{\frac{1}{r_a} + \frac{A}{r_{ac}} + \frac{B}{r_{as}}} \tag{A6}$$

where

$$A = \frac{\Delta + \gamma}{\Delta + \gamma\left(1 + \frac{r_{cw}}{r_{ac}}\right)}, \qquad B = \frac{\Delta + \gamma}{\Delta + \gamma\left(1 + \frac{r_s}{r_{as}}\right)}$$

References

Ashraf, M., Loftis, J., Hubbard, K.G., 1997. Application of geostatistics to evaluate partial weather station networks. Agricultural and Forest Meteorology 84, 255–271.

Beven, K.J., 2001. Rainfall-Runoff Modelling: The Premier, Wiley, Chichester.

Brutsaert, W., 1979. Heat and mass transfer to and from surfaces with dense vegetation or similar permeable roughness. Boundary-Layer Meteorology 16, 365–388.

Canadell, J.R., Jackson, R.B., Ehleringer, J.R., Mooney, H.A., Sala, O.E., Schulze, E.D., 1996. Maximum rooting depth of vegetation types at the global scale. Oecologia 108, 583–595.

Choudhury, B.J., Digirolamo, N.E., 1998. A biophysical process-based estimate of global land surface evaporation using satellite and ancillary data. I. Model description and comparison with observations. Journal of Hydrology 205, 164–185.

Choudhury, B.J., Monteith, J.L., 1988. A four-layer model for the heat budget of homogeneous land surfaces. Quarterly Journal of the Royal Meteorological Society 114, 373–398.

Choudhury, B.J., Rejinatio, R.J., Idso, S.B., 1986. An analysis of infrared temperature observation over wheat and calculations of latent heat flux. Agricultural and Forest Meteorology 37, 75–88.

Choudhury, B.J., Idso, S.B., Rejinato, R.J., 1987. Analysis of an empirical model for soil heat flux under a growing wheat crop for estimating evaporation by an infrared-temperature based energy balance equation. Agricultural and Forest Meteorology 39, 283–297.

Clapp, R.B., Hornberger, G.M., 1978. Empirical equations for some soil hydraulic properties. Water Resources Research 14, 601–604.

Dawes, W.R., Zhang, L., Hatton, T.J., Reece, P.H., Beale, G.T.H., Packer, I., 1997. Evaluation of a distributed parameter ecohydrological model (TOPOG_IRM) on a small cropping rotation catchment. Journal of Hydrology 191, 64–86.

De Ridder, K., Schayes, G., 1997. Radiative transfer in the IAGL land surface model. Journal of Applied Meteorology 36, 12–21.

Famiglietti, J.S., Wood, E.F., 1996. Multiscale modeling of spatially variable water and energy balance processes. Water Resources Research 30, 3061–3078.

Fu, B., Lu, Q., 1990. Atlas of Microclimate Over Shanxi basin, Nanjing University Press, Nanjing, China.

Gao, W., 1995. Parameterization of subgrid-scale land surface fluxes with emphasis on distributing mean atmospheric forcing and using satellite-derived vegetation index. Journal of Geophysical Research 100 (D7), 14305–14317.

Garrat, J.R., Hicks, B.B., 1973. Momentum, heat and water vapour transfer to and from natural and artificial surface. Quarterly Journal of the Royal Meteorological Society 99, 680–687.

Irannejad, P., Shao, Y., 1998. Description and validation of the atmosphere-land-surface interaction scheme (ALSIS) with HAPEX and Cabauw data. Global and Planetary Change 19 (1–4), 87–114.

Jarvis, P.G., 1976. The interpretation of the variation in leaf water potential and stomatal conductance found in canopies in the field. Philosophical Transactions of the Royal Society of London Series B 273, 593–610.

Kergoat, L., 1998. A model for hydrological equilibrium of leaf area index on a global scale. Journal of Hydrology, 212–213.see also pp. 268–286.

Kondo, J., Xu, J., 1997. Seasonal variations in the heat and water balances for nonvegetated surfaces. Journal of Applied Meteorology 36, 1676–1695.

Kustas, W.P., Norman, J.M., 1999. Evaluation of soil and vegetation heat flux predictions using a simple two-source model with radiometric temperatures for partial canopy cover. Agricultural and Forest Meteorology 94, 13–29.

Lhomme, J.P., 1992. Energy balance of heterogeneous terrain: averaging the controlling parameters. Agricultural and Forest Meteorology 61, 11–21.

Liang, X., Lettenmaier, D.P., Wood, E.F., Burges, S.J., 1994. A simple hydrologically based model of land surface water and energy fluxes for general circulation models. Journal of Geophysical Research 99 (D7), 14415–14428.

Liu, S., Mo, X., Leslie, L.M., Speer, M., Bunker, R., Zhao, W., 2001. Another look at the Xinanjiang model: from theory to practice. In: Proceedings of the MODSIM2001 Congress, 10–13 December, Canberra, 137–142.

Maisongrande, P., Ruimy, A., Dedieu, G., Saugier, B., 1995. Monitoring seasonal and interannual variations of gross primary productivity and net ecosystem productivity using a diagnostic model and remotely-sensed data. Tellus 47B, 178–190.

Mauser, W., Schadlich, S., 1998. Modelling the spatial distribution of evapotranspiration on different scales using remote sensing data. Journal of Hydrology, 212–213.see also pp. 250–267.

McVicar, T.R., Jupp, D.L.B., 1999. Estimating one-time-of-day meteorological data from standard daily data as inputs to thermal remote sensing based energy balance model. Agricultural and Forest Meteorolgy 96, 219–238.

Mo, X., Liu, S., 2001. Simulating evapotranspiration and photosynthesis of winter wheat over the growing season. Agricultural and Forest Meteorology 109, 203–222.

Mo, X., Lin, Z., Liu, S., 2000. An improvement of the dual-source model based on Penman–Monteith formula. Journal of Hydraulic Engineering 5, 6–11.in Chinese.

Mo, X., Lin, S., Liu, Z., 2002. Energy balance, water use efficiency and surface resistance in a maize field. Chinese Journal of Applied Ecology 13, 551–554.

Monteith, J.L., 1981. Evaporation and surface temperature. Quarterly Journal of the Royal Meteorological Society 107, 1–27.

Noilhan, J., Planton, S., 1989. A simple parameterization of land surface processes for meteorological models. Monthly Weather Review 117, 536–549.

Norman, J.M., Kustas, W.P., Humes, K.S., 1995. A two-source approach for estimating soil and vegetation energy fluxes from observations of directional radiometric surface temperature. Agricultural and Forest Meteorology 77, 263–293.

Ross, J., 1975. Radiative transfer in plant communities. In: Monteith, J.L., (Ed.), Vegetation and the Atmosphere, Academic Press, London, pp. 13–55.

Sellers, P.J., Mintz, Y., Sud, Y.C., Dalcher, A., 1986. A simple biosphere model (SiB) for use within general circulation models. Journal of Atmospheric Science 43, 305–331.

Sellers, P.J., Heiser, M.D., Hall, F.G., 1992. Relationship between surface conductance and spectral vegetation indices at intermediate ($100\ m^2$–$15\ km^2$) length scales. Journal of Geophysical Research 97 (FIFE Special Issue), 19033–19060.

Sellers, P.J., Los, S.O., Tucker, C.J., Justice, C.O., Dazlich, D.A., Collatz, G.J., Randall, D.A., 1996. A revised land surface parameterization (SiB2) for atmospheric GCMs. Part II. The generation of global fields of terrestrial biophysical parameters from satellite data. Journal of Climate 9, 706–737.

Shuttleworth, W.J., Wallace, J.S., 1985. Evaporation from sparse crops—an energy combination theory. Quarterly Journal of the Royal Meteorological Society 111, 839–855.

Silberstein, R.P., Sivapalan, M., 1995. Modelling vegetation heteorogeneity effects on terrestrial water and energy balances. Environmental International. 21, 477–484.

Silberstein, R.P., Sivapalan, M., Viney, N.R., Held, A., Hatton, T.J., 2003. Modelling the energy balance of a natural jarrah (*Eucalyptus marginata*) forest. Agricultural and Forest Meteorology 115, 201–230.

Singh, V.P., 1995. Computer Models of Watershed Hydrology, Water Resources Publications, Colorado, USA, p. 1130.

Stewart, J.B., 1988. Modelling surface conductance of pine forest. Agricultural and Forest Meteorology 43, 19–35.

Strasser, U., Mauser, W., 1994. Modelling the spatial and temporal variations of the water balance for the Weser catchment 1965–1994. Journal of Hydrology 254, 199–214.

Verseghy, D.L., McFarlance, N.A., Lazare, M., 1993. CLASS—a Canadian land surface scheme for GCMs. II. Vegetation model and coupled runs. International Journal of Climatology 13, 347–370.

Wang, Q., Takahashi, H., 1999. A land surface water deficit model for an arid and semiarid region: impact of desertification on the water deficit status in the Loess Plateau, China. Journal of Climate 12, 244–257.

Wu, C., 1990. 1:1,000,000 Land-Use in Map of China. Science Press, Beijing, China.

Zhao, R.J., 1992. The Xinanjiang model applied in China. Journal of Hydrology 135, 371–381.

Zuo, D., Zhou, Y., Xiang, Y., Zhu, Z., Xie, X., 1991. Studies on Radiation in the Epigeosphere, Science Press, Beijing, China, 26 pp.